


# Concomitant inhibition of the thioredoxin system and nonhomologous DNA repair potently sensitizes Philadelphia-positive lymphoid leukemia to tyrosine kinase inhibitors

Lukasz Komorowski<sup>1,2</sup>  | Agnieszka Dabkowska<sup>1,3</sup> | Joanna Madzio<sup>4</sup> |  
 Agata Pastorczak<sup>4</sup> | Kacper Szczygiel<sup>1,5</sup> | Martyna Janowska<sup>3</sup> | Klaudyna Fidy<sup>1</sup> |  
 Maksymilian Bielecki<sup>6</sup> | Jaromir Hunia<sup>1</sup> | Malgorzata Bajor<sup>3</sup> | Tomasz Stoklosa<sup>7</sup> |  
 Magdalena Winiarska<sup>1,3</sup> | Elzbieta Patkowska<sup>8</sup> | Malgorzata Firczuk<sup>1,3</sup>

Correspondence: Malgorzata Firczuk (mfirczuk@imdik.pan.pl)

## Abstract

Breakpoint cluster region-Abelson (*BCR::ABL1*) gene fusion is an essential oncogene in both chronic myeloid leukemia (CML) and Philadelphia-positive (Ph<sup>+</sup>) B-cell acute lymphoblastic leukemia (B-ALL). While tyrosine kinase inhibitors (TKIs) are effective in up to 95% of CML patients, 50% of Ph<sup>+</sup> B-ALL cases do not respond to treatment or relapse. This calls for new therapeutic approaches for Ph<sup>+</sup> B-ALL. Previous studies have shown that inhibitors of the thioredoxin (TXN) system exert antileukemic activity against B-ALL cells, particularly in combination with other drugs. Here, we present that peroxiredoxin-1 (PRDX1), one of the enzymes of the TXN system, is upregulated in Ph<sup>+</sup> lymphoid as compared to Ph<sup>+</sup> myeloid cells. PRDX1 knockout negatively affects the viability of Ph<sup>+</sup> B-ALL cells and sensitizes them to TKIs. Analysis of global gene expression changes in imatinib-treated, PRDX1-deficient cells revealed that the nonhomologous end-joining (NHEJ) DNA repair is a novel vulnerability of Ph<sup>+</sup> B-ALL cells. Accordingly, PRDX1-deficient Ph<sup>+</sup> B-ALL cells were susceptible to NHEJ inhibitors. Finally, we demonstrated the potent efficacy of a novel combination of TKIs, TXN inhibitors, and NHEJ inhibitors against Ph<sup>+</sup> B-ALL cell lines and primary cells, which can be further investigated as a potential therapeutic approach for the treatment of Ph<sup>+</sup> B-ALL.

## INTRODUCTION

Philadelphia chromosome (Ph) results from a reciprocal translocation t(9;22)(q34;q11), leading to the expression of a constitutively active breakpoint cluster region-Abelson (*BCR-ABL1*) tyrosine kinase.<sup>1</sup> While this genetic aberration is a hallmark of chronic myeloid leukemia (CML),<sup>1</sup> Ph is also detected in up to 4% of pediatric and 50% of adult cases of B-cell acute lymphoblastic leukemia (B-ALL).<sup>2,3</sup> Even though CML and Ph-positive B-ALL (Ph<sup>+</sup> B-ALL) share the same driver

oncogenic aberration, their clinical outcomes are substantially different. CML in a chronic phase (CP) responds to treatment in up to 95% of cases due to the introduction of tyrosine kinase inhibitors (TKIs), which block the activity of *BCR::ABL1*. In up to 5% of cases, CML cells acquire secondary genetic lesions that may lead to a blastic phase (BP) of either myeloid (myBP, approximately 70% of cases) or lymphoid (lyBP) lineage. LyBP CML phenotypically and metabolically resembles Ph<sup>+</sup> B-ALL.<sup>1,4-6</sup> Although treatment protocols for Ph<sup>+</sup> lymphoid leukemia include TKIs in combination with multiagent

<sup>1</sup>Department of Immunology, Medical University of Warsaw, Warsaw, Poland

<sup>2</sup>Postgraduate School of Molecular Medicine, Medical University of Warsaw, Warsaw, Poland

<sup>3</sup>Laboratory of Immunology, Mossakowski Medical Research Institute, Polish Academy of Sciences, Warsaw, Poland

<sup>4</sup>Department of Pediatrics, Oncology and Hematology, Medical University of Lodz, Lodz, Poland

<sup>5</sup>Polpharma Biologics SA, Gdańsk, Poland

<sup>6</sup>Department of Psychology, SWPS University of Social Sciences and Humanities, Warsaw, Poland

<sup>7</sup>Department of Tumor Biology and Genetics, Medical University of Warsaw, Warsaw, Poland

<sup>8</sup>Institute of Hematology and Transfusion Medicine, Warsaw, Poland

This is an open access article under the terms of the [Creative Commons Attribution-NonCommercial-NoDerivs](https://creativecommons.org/licenses/by-nc-nd/4.0/) License, which permits use and distribution in any medium, provided the original work is properly cited, the use is non-commercial and no modifications or adaptations are made.

© 2024 The Authors. *HemaSphere* published by John Wiley & Sons Ltd on behalf of European Hematology Association.

chemotherapy, the probability of a 5-year overall survival of patients is less than 50%.<sup>7</sup> This represents an unmet clinical need to find better therapeutic strategies for Ph<sup>+</sup> B-ALL.

One of the potential vulnerabilities of Ph<sup>+</sup> B-ALL results from dysregulated redox homeostasis. Inducible expression of *BCR::ABL1* in pro-B-cell line models was shown to elevate H<sub>2</sub>O<sub>2</sub> levels.<sup>8,9</sup> Moreover, according to previous reports, patients suffering from B-ALL show increased levels of circulating oxidative stress markers.<sup>10</sup> Constant oxidative stress in leukemic cells must be counterbalanced by some compensatory mechanism, allowing cells to prevent apoptosis caused by excessive oxidative damage. Such a major antioxidant role in B-cell malignancies has been already attributed to the thioredoxin (TXN) system.<sup>10–12</sup> Its elements, TXN, TXN reductase (TXN-R), and peroxiredoxin (PRDX), were shown to be upregulated in various subtypes of B-ALL.<sup>10</sup> Among the various compounds known to inhibit the TXN system, auranofin (AUR) is the only clinically available drug. Primarily approved for rheumatoid arthritis, AUR has displayed remarkable anti-tumor characteristics and is now extensively tested as a putative antitumor agent in preclinical and clinical studies (NCT01737502).<sup>13,14</sup> Although alternative molecular targets have been associated with the anticancer effects of AUR,<sup>15,16</sup> it is widely believed that TXN-R is the primary target at the low micromolar concentration range.<sup>17–19</sup> Notably, AUR showed promising antitumor effects in various B-cell malignancies,<sup>11,12</sup> including B-ALL.<sup>10</sup> However, the importance of these observations in Ph<sup>+</sup> B-ALL has not been confirmed yet.

Increased oxidative and proliferative stress may also lead to the accumulation of potentially lethal DNA damage, especially double-strand breaks (DSBs),<sup>20</sup> which induce DNA damage response (DDR). The main DDR pathways responsible for DSB repair are homologous recombination (HR), and nonhomologous end-joining (NHEJ), which can be further divided into classical and alternative NHEJ (cNHEJ and altNHEJ, respectively).<sup>21</sup> Previous studies have shown that *BCR::ABL1* can affect DDR pathways. For example, two key HR and cNHEJ proteins—breast cancer type 1 susceptibility protein (BRCA1) and DNA-dependent protein kinase (DNA-PK), respectively, are downregulated in CML cells.<sup>22,23</sup> Interestingly, even though inhibition of *BCR::ABL1* by imatinib (IMAT), a first-generation TKI, partially restored expression of BRCA1 and DNA-PK, it downregulated other core proteins required for HR (RAD51) or cNHEJ (ligase 4).<sup>24,25</sup> This indicated the potential use of the synthetic lethality approach in Ph<sup>+</sup> leukemias, as they seem to be heavily dependent on altNHEJ.<sup>26</sup> This notion was further confirmed by promising results of combining IMAT with altNHEJ inhibitor olaparib (OLAP) in CML.<sup>26</sup> However, cNHEJ targeting has been studied neither in CML nor in Ph<sup>+</sup> B-ALL. Notably, recent findings suggest that SUP-B15, a Ph<sup>+</sup> B-ALL cell line, relies mainly on cNHEJ to repair doxorubicin-induced DSBs.<sup>27</sup> This suggests a prominent role of cNHEJ in Ph<sup>+</sup> B-ALL cells. However, more in-depth studies are needed, as detailed gene expression analysis of DDR pathways and therapeutic assessment of targeting DDR have not yet been performed in Ph<sup>+</sup> B-ALL.

In this work, we investigated the role of the TXN system in Ph<sup>+</sup> B-ALL to identify more effective therapeutic approaches for this leukemia subtype. We showed that PRDX1, a member of the TXN system, plays a growth-supporting role in Ph<sup>+</sup> lymphoid leukemias. Investigation of PRDX1-deficient Ph<sup>+</sup> lymphoid cells revealed decreased viability, increased sensitivity to TKIs, and higher accumulation of DNA damage. We also showed that lymphoid cells lacking PRDX1 are more susceptible to NHEJ inhibition and that either PRDX1 silencing or the TXN system inhibition by AUR greatly improved the effectiveness of TKIs. Finally, we demonstrated the in vitro antileukemic efficacy of the triple combination consisting of clinically relevant concentrations of TKIs, cNHEJ, and TXN system inhibitors, both in Ph<sup>+</sup> lymphoid cell lines and in patient-derived Ph<sup>+</sup> B-ALL cells.

## MATERIALS AND METHODS

### Cell culture

Ph<sup>+</sup> human cell lines representing myeloid (K562, LAMA-84, MEG-A2) or lymphoid (BV173, SUP-B15, TOM-1) lineages were purchased from DSMZ. BV173, SUP-B15, TOM1, K562, and LAMA-84 cells were maintained in RPMI-1640 medium (Gibco), supplemented with either 10% (BV173, K562, LAMA-84) or 20% (TOM1, SUP-B15) fetal bovine serum (FBS) (HyClone) and 1% penicillin/streptomycin (P/S). MEG-A2 cells were cultured in Iscove's modified Dulbecco's medium (Gibco), supplemented with 20% FBS (HyClone) and 1% P/S. All cell lines were kept in a humidified atmosphere at 37°C and 5% CO<sub>2</sub> and routinely checked for Mycoplasma contamination.

### Assessment of changes in gene expression by RNAseq in IMAT-treated BV173 cells

Control (sgNTC) or PRDX1-deficient (sgPRDX1) BV173 cells ( $0.2 \times 10^6$ /mL density) were cultured for 12 or 24 h with or without 250 nM IMAT. Presented timepoints and IMAT concentrations were chosen according to a pilot assessment of cell viability and *BIM* messenger RNA (mRNA) levels by quantitative PCR, choosing conditions that allowed for the survival of at least 50% of cells and an increase in *BIM* transcript levels (data not shown). Total RNA was extracted and assessed for quality, as described in Supporting Information S1: **Methods**. RNA-sequencing was performed using Illumina® Stranded mRNA Prep, Ligation (Illumina) according to the manufacturer's protocol. The procedure as well as statistical analysis are described in Supporting Information S1: **Methods**. Additional analyses of the transcriptomic data were done with the GenePattern platform (Dana Farber) and gene set enrichment analysis (GSEA4.1.0; <https://software.broadinstitute.org/gsea/>) to further explore biological processes and signaling pathways between groups, based on the h.all.v7.4 (hallmark gene sets) and c2.cp.v7.4 (canonical pathways). The cut-off criterion for GSEA was  $p < 0.05$ . Data visualizations and gene clustering were performed in MultiExperiment Viewer software. Pathway enrichment analyses and visualization were carried out with the Enrichment Map (Cytoscape 3.8.2) tool that organizes gene sets into a similarity network by grouping similar gene sets as defined by the number of overlapping genes. The groups of pathways were annotated using the MCL Cluster algorithm based on the similarity coefficient.

### Generation of PDX in NSG mice

For generation of patient-derived xenografts (PDXs), lymphoblasts were isolated from pediatric and adult Ph<sup>+</sup> leukemic patients' bone marrow. Patients' material was obtained from the Institute of Hematology and Blood Transfusion in Warsaw, Poland, and the Central Clinical Hospital of the Medical University of Lodz, following informed written consent, in accordance with the Declaration of Helsinki and the guidelines for good clinical practice. All protocols were approved by the local Bioethics Committee of Medical University of Warsaw: KB/44/2015 and the Medical University of Lodz: RNN/51/19/KE. A summary of patients' characteristics is provided in Supporting Information S1: Table 1. All patients were stratified into a high-risk group.

Transgenic immunodeficient NSG (NOD scid gamma, NOD.Cg-Prkdc<sup>scid</sup> Il2rg<sup>tm1Wjl</sup>/SzJ) mice used for PDX generation were purchased from Charles River Laboratories. In vivo procedures were in accordance with the permission given by the II Local Ethics Committee for Animal Research based at Warsaw University of Life

Sciences (WAW2/095/2019). All mice were kept in specific pathogen-free standard animal facilities, in individually ventilated cages. For the generation of PDX, blasts isolated from six Ph<sup>+</sup> B-ALL or lyBP CML patients' bone marrow were used. These blasts were propagated in NSG mice, as described in Fidyt et al.<sup>10</sup> and in Supporting Information S1: [Methods](#).

## Ex vivo assessment of drug cytotoxicity against PDX cells

Fresh or cryopreserved PDX samples propagated in NSG mice were used for the assessment of ex vivo drug cytotoxicity. For frozen samples whose viability after thawing was less than 90%, dead cells were discarded through centrifugation in the Lymphoprep (STEMCELL Technologies) gradient. Cells were seeded onto a 96-well U-bottom plate at  $0.5 \times 10^6$  cells/mL in a final volume of 200  $\mu$ L of SFEM II medium (Gibco), supplemented with 20% FBS (Gibco), 20 ng/mL recombinant human interleukin-3 and 10 ng/mL recombinant human interleukin-7 (R&D Systems), and cultured with drugs for 72 h. The percentage of viable cells was assessed by flow cytometry (LSRFortessa X-20; BD Biosciences) after staining with propidium iodide (PI) at a final concentration of 1  $\mu$ g/mL.

## Statistical analysis

Data visualization and statistical analysis were performed using the R programming environment.<sup>28</sup> All statistical tests were preceded by screening for outliers and verifying the normality of residuals' distribution. If applicable, two- or three-way analysis of variance (ANOVA) and pairwise *t*-tests were used. All ANOVAs were estimated using heteroscedasticity-consistent standard errors (White correction). If assumptions were violated, comparisons were performed using the Mann-Whitney test. Detailed results of all statistical analyses are described in figure legends and are provided in Supporting Information: [Tables](#).

## RESULTS

### PRDX1 is expressed at high levels in Ph<sup>+</sup> lymphoid cells and supports the maintenance of these cells

We have previously found the upregulation of the elements of the TXN system in various B-ALL subtypes.<sup>10</sup> To further explore this phenomenon in Ph<sup>+</sup> leukemias, we determined the mRNA levels of *TXN1*, *TXN-R1*, and *PRDX1* in primary leukemic cells isolated from patients suffering from Ph<sup>+</sup> myeloid (CP CML, myBP CML) or lymphoid (lyBP CML or Ph<sup>+</sup> B-ALL) leukemias. In the myeloid cells, the mRNA levels of *PRDX1* were relatively low, independent of the phase of the disease (Figure 1A). In comparison to myeloid cells, in the Ph<sup>+</sup> lymphoid cells *PRDX1* expression was significantly higher (Figure 1A). Similarly, *PRDX1* protein levels were higher in Ph<sup>+</sup> lymphoid cell lines as compared to myeloid ones (Figure 1B). In contrast, *TXN1* and *TXN-R1* mRNA levels were lower in Ph<sup>+</sup> leukemic cells of lymphoid origin (Supporting Information S1: Figure 1A). However, the *TXN1* protein levels varied across the Ph<sup>+</sup> cell lines (Supporting Information S1: Figure 1B). To confirm our observations in large patient cohorts, we analyzed publicly available expression datasets of diverse myeloid and lymphoid malignancies as well as healthy bone marrow (EGAS00001003266, GSE13204). Ph<sup>+</sup> B-ALL cells and other B-ALL subtypes showed higher *PRDX1* mRNA levels than healthy bone marrow and other hematological malignancies

(CML, AML, T-ALL, CLL) (Supporting Information S1: Figure 2 and Supporting Information S2: Tables 2 and 3). Additionally, Ph<sup>+</sup> B-ALL cells exhibited lower *TXN1* and *TXN-R1* mRNA levels compared to healthy bone marrow and many other hematological malignancies (Supporting Information S1: Figure 2 and Supporting Information S2: Tables 2 and 3), confirming the experimental findings presented in Figure 1.

These results led us to hypothesize that *PRDX1* may play a significant role in Ph<sup>+</sup> lymphoid malignancies. To investigate this assumption, we obtained myeloid (K562) and lymphoid (BV173) cell lines with CRISPR-Cas9-mediated genomic *PRDX1* knockout (sg*PRDX1*) confirmed by immunoblotting (Figure 1C, Supporting Information S1: Figure 3A). We observed that *PRDX1* deletion reduced the numbers of viable BV173 cells grown in vitro (Figure 1D and Supporting Information S1: Table 4), while it did not affect K562 cell numbers (Supporting Information S1: Figure 3B and Table 5). As the main catalytic role of *PRDX1* is the removal of H<sub>2</sub>O<sub>2</sub>, we investigated the impact of reactive oxygen species (ROS) on the observed effect in BV173 cells. As presented in Figure 1D, the addition of ROS scavengers to the culture medium restored the numbers of viable BV173 cells, indicating that the reduction of viable cells by the *PRDX1* knockout in BV173 cells is ROS-dependent. All the above results suggest that the role of *PRDX1* in supporting cell maintenance is restricted to Ph<sup>+</sup> lymphoid leukemias.

### Inhibition of the TXN system sensitizes Ph<sup>+</sup> lymphoid cell lines to TKIs

To investigate how pharmacological inhibition of *PRDX1* affects the sensitivity of Ph<sup>+</sup> cells to TKIs, we employed AUR, which indirectly blocks *PRDX1* via inhibition of TXN-R, and adenanthin (ADE), a direct inhibitor of *PRDX1* and other elements of the TXN system.<sup>29</sup> AUR potently and dose-dependently enhanced the cytotoxic effects of IMAT and dasatinib (DASA) in Ph<sup>+</sup> lymphoid cell lines (BV173 and SUP-B15). When the interactions between AUR and TKIs were calculated using the SynergyFinder R package,<sup>30</sup> strong synergistic effects were seen at higher drug concentrations, as visualized by the synergy scores (Synergy Score > 10 means synergistic effect) (Figure 2A). In contrast, AUR did not significantly enhance the cytotoxic effects of TKIs in Ph<sup>+</sup> myeloid cell lines K562 and MEG-A2 (Supporting Information S1: Figure 4). Similarly, ADE potentiated the cytotoxicity of TKIs specifically in Ph<sup>+</sup> lymphoid cell lines (Supporting Information S1: Figure 5A,B).

### PRDX1 knockout potently sensitizes Ph<sup>+</sup> lymphoid cells to TKIs

As pharmacological inhibition of the TXN system augmented the cytotoxicity of TKIs in lymphoid cells, we next checked the effect of the *PRDX1* knockout in lymphoid (BV173) and myeloid (K562) cells on their sensitivity to TKIs. BV173 cells lacking *PRDX1* were more sensitive to IMAT, DASA, and ponatinib (PONA) in all tested concentrations (Figure 2B and Supporting Information S1: Table 6). In contrast, no sensitization to TKIs by the *PRDX1* knockout was observed in myeloid K562 cells (Supporting Information S1: Figure 6 and Table 7). We also checked whether the sensitization of lymphoid *PRDX1*-knockout cells to IMAT could be maintained over a longer time. In a 6-day clonogenic assay, the overall number of colony-forming units (CFUs) was much lower for the untreated sg*PRDX1* cells in comparison to the untreated control cells (Supporting Information S1: Figure 7). Furthermore, the number of CFUs of IMAT-treated cells relative to

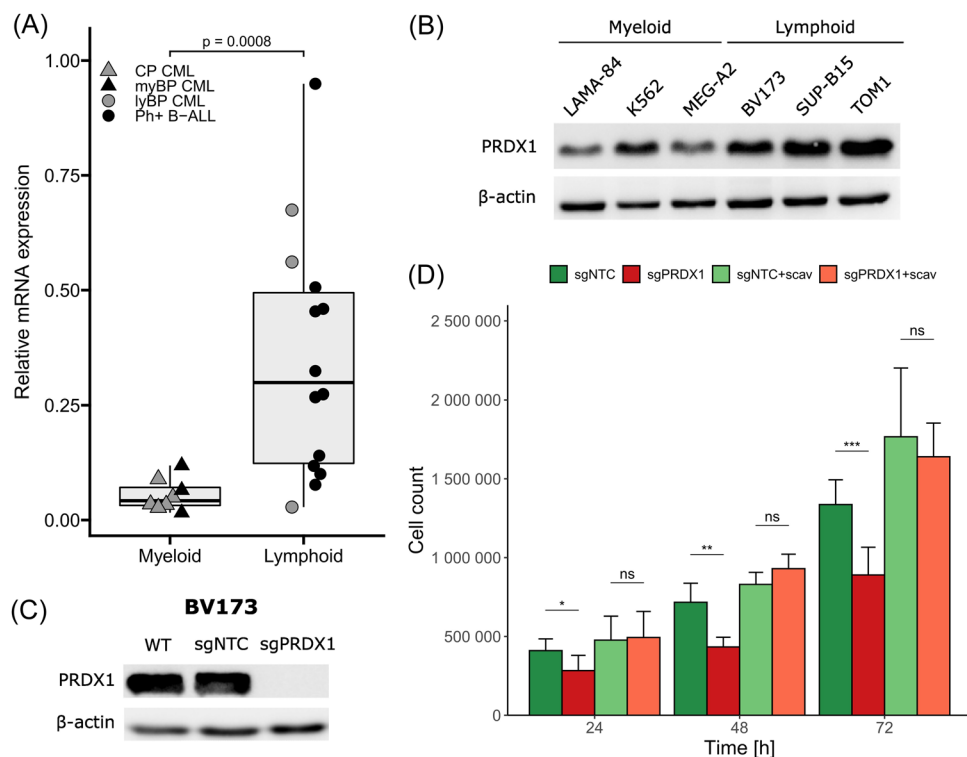


**FIGURE 1** Peroxiredoxin 1 (PRDX1) is upregulated in Philadelphia-positive (Ph<sup>+</sup>) lymphoid cells and plays an important role in their maintenance. (A) Relative PRDX1 messenger RNA levels in primary cells isolated from the bone marrow of leukemic patients: chronic myeloid leukemia in chronic phase (CP CML,  $n = 5$ ), CML in myeloid blast phase (CML myBP,  $n = 3$ ), CML in lymphoid blast phase (CML lyBP,  $n = 3$ ), and Ph<sup>+</sup> B-cell acute lymphoblastic leukemia (B-ALL) ( $n = 11$ ). *RPL29* was used as a reference gene. Medians with first and third quartiles  $\pm$  interquartile ranges are presented. Statistical significance was evaluated using the Mann-Whitney test. (B) PRDX1 levels in Ph<sup>+</sup> cell lines were assessed by immunoblotting. (C) Confirmation of the genomic knockout of PRDX1 in BV173 cells by immunoblotting. (D) Evaluation of the numbers of BV173 viable cells by light microscope counting after discriminating dead cells with Trypan Blue staining, for 3 consecutive days of in vitro culture. Two groups had reactive oxygen species scavengers (scav) added to the culture media at the start of the experiment: 50  $\mu$ g/mL catalase, and 1 mM sodium pyruvate. Means  $\pm$  SD are presented ( $n = 6$ ). Statistical significance was estimated by a two-way analysis of variance followed by post hoc pairwise *t*-tests for cells without or with scavengers performed separately. ns, Not significant. \* $p < 0.05$ ; \*\* $p < 0.01$ ; \*\*\* $p < 0.001$ .

control groups was significantly lower for the cells with PRDX1 knockout (Figure 2C), indicating that the sensitization of PRDX1-knockout lymphoid cells to IMAT was found to persist for a longer period of time. Investigation of the changes in cell death signaling pathways in IMAT-treated cells upon PRDX1 knockout revealed an overactivation of c-Jun N-terminal kinase, increased amounts of proapoptotic Bcl-2 interacting mediator of cell death (BIM), decreased amounts of anti-apoptotic B-cell lymphoma-W (BCL-W), and enhanced induction of apoptosis manifested by increased cleavage of caspase-3 and poly (ADP-ribose) polymerase 1 (PARP1; Figure 2D). These results indicate that the knockout of PRDX1 in BV173 cells sensitizes them to TKIs and potentiates TKI-induced apoptosis.

### PRDX1 knockout causes global transcriptome changes upon IMAT treatment

To better understand the mechanism of sensitization to TKIs by a PRDX1 knockout, we performed transcriptome analysis by RNA sequencing of both control (sgNTC) and PRDX1-deficient (sgPRDX1) BV173 cells, untreated or treated with 250 nM IMAT for 12 and 24 h (GEO accession number GSE221906; three-dimensional principal component analysis presented in Supporting Information S1: Figure 8).

First, we compared gene expression in untreated control and sgPRDX1 cells and found that the PRDX1 knockout resulted in at

least a twofold significant change in 58 genes (Supporting Information S1: Table 8). Out of 42 downregulated genes, some have recognized leukemia-promoting functions, such as stimulation of proliferation (*IRF8*,<sup>31</sup> *PRAME*,<sup>32</sup> *APOC4-APOC2*<sup>33</sup>), stemness (*CYBB*,<sup>34</sup> *BMPR1A*<sup>35</sup>), survival (*ANXA5*,<sup>36</sup> *H19*<sup>37</sup>), promotion of oncogenesis (*MLF1*<sup>38</sup>), and drug resistance (*CASD1*,<sup>39</sup> *SPARC*<sup>40</sup>). Among the 16 upregulated genes, we found tumor suppressors (*LRRC26*,<sup>41</sup> *SRCIN1*<sup>42</sup>). To investigate the effects of PRDX1 knockout on gene expression profiles, we performed GSEA, comparing untreated sgPRDX1 and sgNTC cells (Supporting Information S1: Figure 9 and Supporting Information S2: Tables 9 and 10). The most notable changes were activation of the pathways connected to DNA damage and cell cycle checkpoints, signal transduction, and both NOTCH and RAS signaling. We also observed suppression of pathways related to metabolic activation (oxidative phosphorylation, translation). These observations support our hypothesis on the protective role of PRDX1 in maintenance and survival of BV173 cells.

To gain more insight into early (12 h of IMAT treatment) and late (24 h of IMAT treatment) changes in gene expression profiles, we performed GSEA, comparing IMAT-treated sgPRDX1 with IMAT-treated sgNTC cells in two timepoints. Numerous gene sets were found to be significantly dysregulated (false discovery rate < 0.05) after PRDX1 knockout, with 86 upregulated and 188 downregulated gene sets after 12 h of IMAT treatment (Supporting Information S2: Table 11), and 175 upregulated and 48 downregulated gene sets after 24 h of exposure to



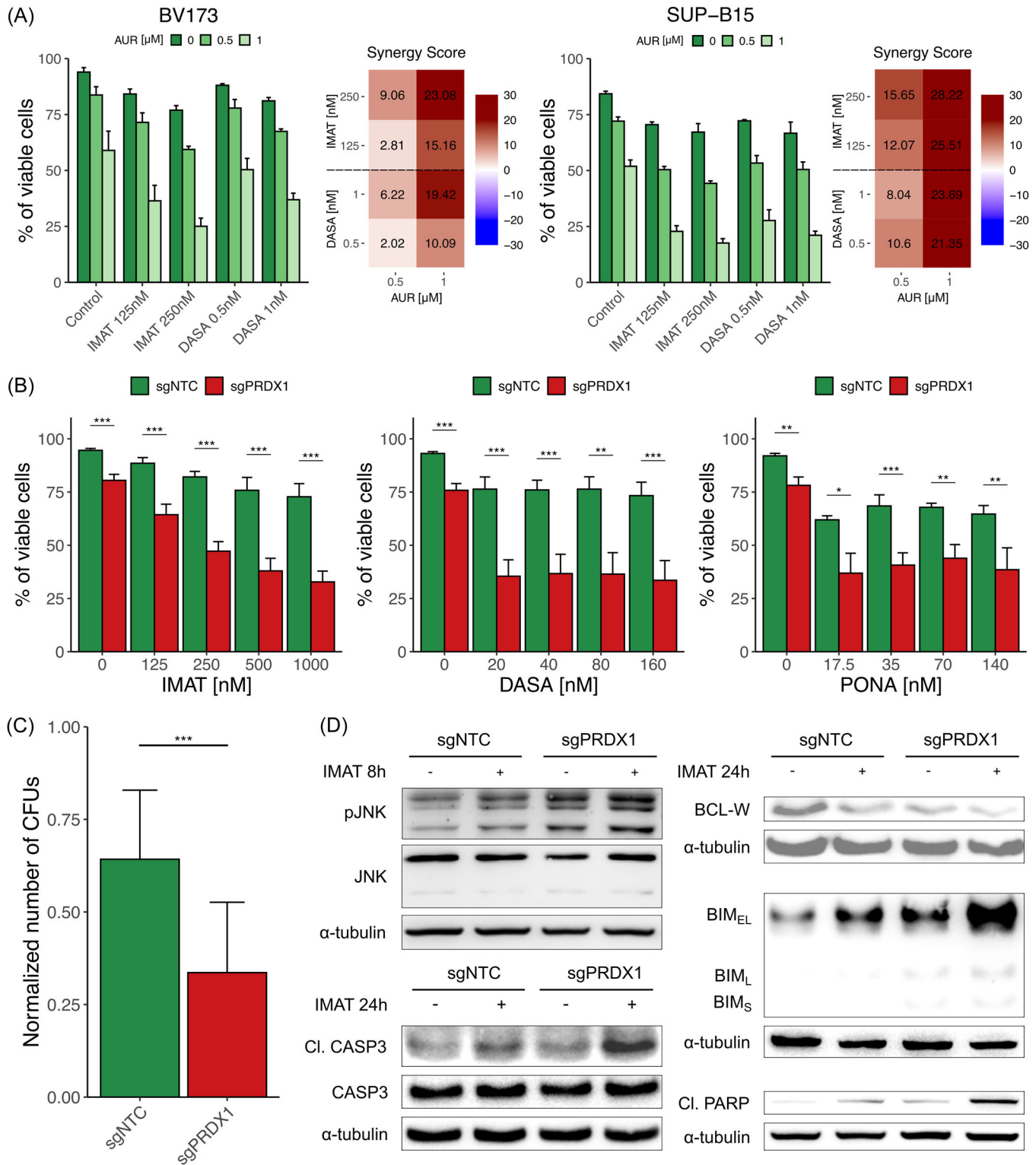


**FIGURE 2** Thioredoxin (TXN) system inhibition as well as *peroxiredoxin-1* (PRDX1) knockout sensitizes Philadelphia-positive (Ph<sup>+</sup>) B-cell acute lymphoblastic leukemia (B-ALL) cells to tyrosine kinase inhibitors (TKIs). (A) The viability of lymphoid Ph<sup>+</sup> cell lines, BV173 ( $n = 4$ ), and SUP-B15 ( $n = 3$ ), treated with indicated concentrations of drugs for 48 h, was assessed by the propidium iodide (PI) staining and flow cytometry. Means  $\pm$  SD are presented. Bliss synergy scores are presented next to the corresponding plots. (B) The viability of BV173 cells treated with TKIs for 48 h was assessed by propidium iodide (PI) staining and flow cytometry. Means  $\pm$  SD are presented (imatinib [IMAT]  $n = 8$ , dasatinib [DASA]  $n = 4$ , ponatinib [PONA]  $n = 4$ ). Statistical significance was estimated by a two-way analysis of variance followed by post hoc pairwise  $t$ -tests. \* $p < 0.05$ ; \*\* $p < 0.01$ ; \*\*\* $p < 0.001$ . (C) Normalized colony forming units number of BV173 cells that were treated for 2 h with 1000 nM IMAT and subsequently grown for 6 days in a culture medium with methylcellulose. Means normalized to controls  $\pm$  SD are presented (sgNTC  $n = 7$ , sgPRDX1  $n = 8$ ). Statistical significance was estimated by Welch's two-sample  $t$ -test. \*\*\* $p < 0.01$ . (D) Amounts of apoptosis-related proteins in control and IMAT-treated BV173 sgPRDX1 cells in comparison to the control sgNTC cells were measured by immunoblotting. Times of incubation with IMAT are indicated above the blots.  $\alpha$ -Tubulin was used as a loading control.

IMAT (Supporting Information S2: Table 12). Most significantly changed functional clusters of pathways in sgPRDX1 cells after 12 h of IMAT treatment included downregulation of genes involved in translation and transcription regulation, oxidative phosphorylation, or amino acid synthesis, indicating suppression of cellular metabolism. Notably, in sgPRDX1 cells incubated with IMAT for 12 h, we observed the upregulation of pathways involved in DNA repair and phosphoinositide 3-kinase signaling (Figure 3A and Supporting Information S2: Table 13). Among the unclustered gene sets upregulated in sgPRDX1 cells after 12 h of IMAT treatment, we found pathways related to oxidative stress (Figure 3A, right panel and Supporting Information S2: Table 11). Late changes observed after 24 h of IMAT treatment induced the upregulation of two major gene set clusters in sgPRDX1 cells, linked to apoptosis

and signal transduction (Figure 3B and Supporting Information S2: Table 14). Moreover, we observed the upregulation of several DDR pathways (Figure 3B and Supporting Information S2: Table 14). Among gene sets that did not fit in any cluster, we identified two related to P53 signaling and oxidative stress response (Figure 3B, right panel and Supporting Information S2: Table 12). Additional GSEA analyses evaluating the IMAT effect in sgPRDX1 cells are presented in Supporting Information S2: Tables 15 and 16. Collectively, the results of the GSEA analysis and gene sets clustering indicate that in early response to IMAT, loss of PRDX1 leads to the slowdown of metabolism, while after longer exposition to IMAT, it results in increased cell death. Notably, at both timepoints we observed the activation of pathways involved in DDR.

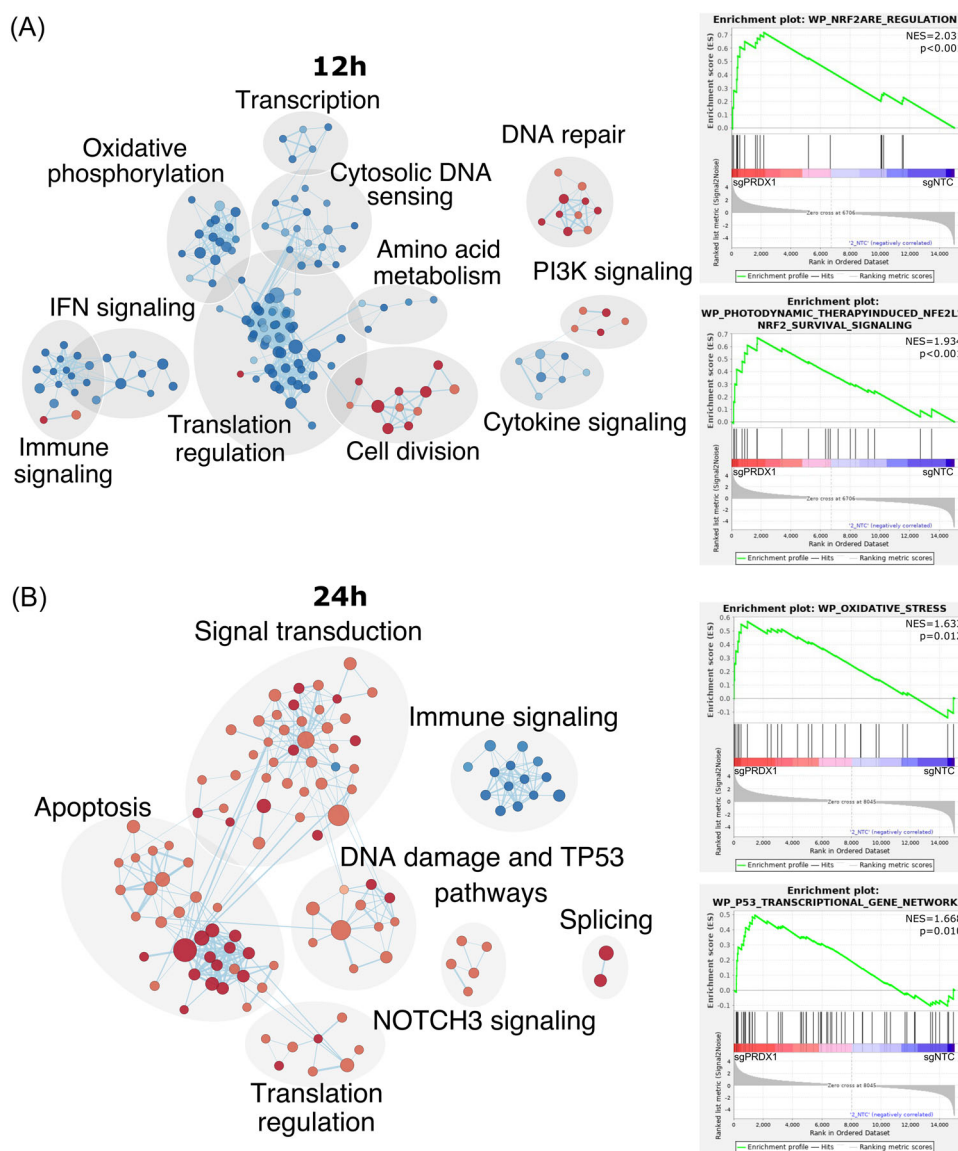


**FIGURE 3** Global changes in gene expression pathways in *peroxiredoxin-1* (*PRDX1*)-knockout and imatinib (IMAT)-treated BV173 cells. Functional clustering of IMAT-induced pathways significantly upregulated (red) or downregulated (blue) upon *PRDX1* knockout in BV173 cells. The pathways were identified by the gene set enrichment analysis (GSEA) of differentially expressed genes in sgPRDX1 and sgNTC cells after 12 h (panel A) or 24 h (panel B) of 250 nM IMAT treatment. Each node represents a different pathway. The size of the node corresponds to the size of the gene set. The thickness of lines between nodes depicts the number of convergent genes between the two gene sets. Selected enrichment plots not fitting any of the clusters within each timepoint are also presented. On both panels, there are also presented GSEA plots for pathways that did not fit any of the clusters but were significantly upregulated in sgPRDX1 cells in comparison to sgNTC cells (false discovery rate < 0.05).

## Canonical functions of PRDX1 do not fully explain the sensitization of the PRDX1 knockout to TKIs

Consistent with the well-known role of PRDX1 in removing ROS and the documented role of the TXN system elements in the prevention of the endoplasmic reticulum stress and ROS accumulation,<sup>10,43</sup> in IMAT-treated, PRDX1-deficient cells, we found the upregulation of pathways associated with ER and oxidative stress. Therefore, we investigated the significance of ROS in the sensitization of BV173 cells to IMAT by the PRDX1 deletion. To this end, we reconstituted WT PRDX1 and its catalytically active (C83A) and inactive (C52A, C173A) point-mutated variants<sup>44,45</sup> in BV173 sgPRDX1 cells and checked their sensitivity to IMAT. As presented in Figure 4A, all PRDX1 variants were expressed in BV173 at levels similar to parental cells. The higher molecular weight of the reconstituted PRDX1

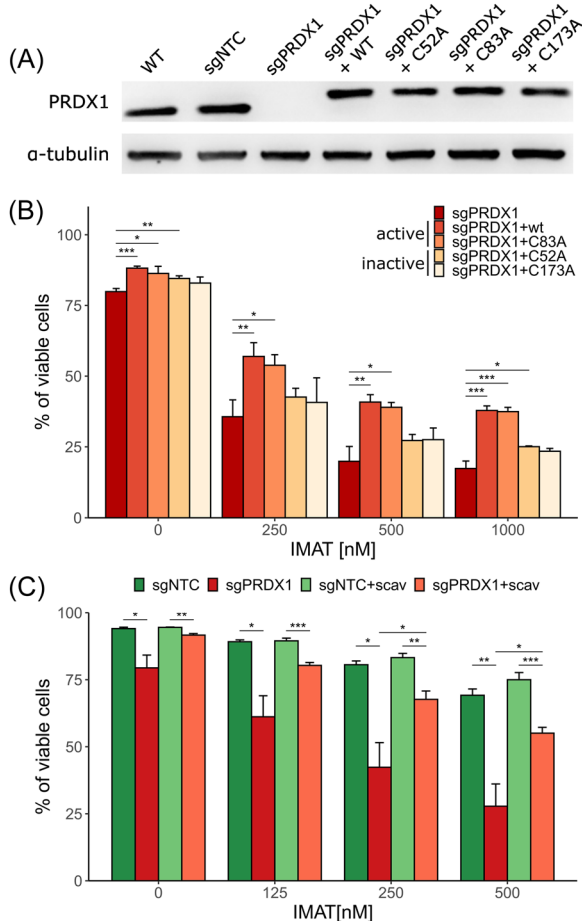


**FIGURE 4** Reactive oxygen species (ROS) scavenging by peroxiredoxin-1 (PRDX1) contributes to the sensitization of the PRDX1-knockout cells to tyrosine kinase inhibitors (TKIs). (A) Confirmation of PRDX1 variants reconstitution in BV173 sgPRDX1 cells by immunoblotting. (B) Sensitivity of sgPRDX1 BV173 cells expressing wild-type PRDX1 or its mutated variants to imatinib (IMAT). Means  $\pm$  SD are presented ( $n = 4$ ). Statistical significance was estimated by a two-way analysis of variance (ANOVA) followed by post hoc pairwise t-tests with Bonferroni correction, treating sgPRDX1 cells as a reference and computed for each IMAT concentration separately. \* $p < 0.05$ ; \*\* $p < 0.01$ ; \*\*\* $p < 0.001$ . (C) Sensitivity of BV173 cells to IMAT in the presence of ROS scavengers. Means  $\pm$  SD are presented ( $n = 4$ ). Statistical significance was estimated by a two-way ANOVA with post hoc pairwise t-tests with Bonferroni correction computed for each IMAT concentration. \* $p < 0.05$ ; \*\* $p < 0.01$ ; \*\*\* $p < 0.001$ .

variants is due to the presence of the approximately 2 kDa T2A linker. The expression of catalytically active PRDX1 (WT or C83A) significantly reversed the effect of the PRDX1 knockout on the sensitivity to IMAT, while the inactive mutants improved cell viability only slightly (Figure 4B and Supporting Information S1: Table 17). Accordingly, the addition of ROS scavengers to the cell culture medium improved sgPRDX1 cells' viability upon IMAT treatment, although not to the level of sgNTC cells (Figure 4C and Supporting Information S1: Table 18). Surprisingly, intracellular levels of ROS (Supporting Information S1: Figure 10A–C and Supporting Information S1: Tables 19–21) and extracellular oxidative stress marker 8-hydroxydeoxyguanosine (Supporting Information S1: Figure 10D and Table 22) did not show any significant differences between sgNTC and sgPRDX1 cells. These results indicate that the canonical, ROS-scavenging function of PRDX1 plays an important role in the sensitization of the PRDX1-knockout cells to TKIs; however, it does not fully explain the observed effects. Therefore, we further searched for other mechanisms involved in the process of sensitization.

## Knockout of PRDX1 leads to the upregulation of DDR-related pathways and the accumulation of DNA damage

As RNAseq analysis revealed the upregulation of DDR pathways in BV173 sgPRDX1 cells at both timepoints of IMAT treatment (Figure 5A), we investigated the degree of DNA damage upon PRDX1 knockout. Treatment of BV173 sgPRDX1 cells with IMAT resulted in a greater accumulation of DNA lesions as compared with sgNTC cells, as demonstrated by measuring H2AX phosphorylation (Figure 5B,C and Supporting Information S1: Table 23) and the terminal deoxynucleotidyl transferase dUTP nick-end labeling (TUNEL) assay (Figure 5D and Supporting Information S1: Table 24). These results indicate that the transcriptional upregulation of DDR pathways is insufficient to counterbalance the accumulation of DNA damage in PRDX1-knockout cells. Hence, we conclude that DDR pathways might be an exploitable vulnerability of Ph<sup>+</sup> lymphoid cells with deleted or pharmacologically blocked PRDX1.

## Concomitant inhibition of the TXN system and the NHEJ pathways significantly improves the cytotoxicity of TKIs in Ph<sup>+</sup> lymphoid cells

To evaluate whether PRDX1 plays a role in the sensitivity to NHEJ inhibitors, we treated sgNTC and sgPRDX1 cells with inhibitors of cNHEJ (nedisertib—NEDI) or altNHEJ (OLAP). In BV173, the deletion of PRDX1 caused increased sensitivity to both NHEJ inhibitors (Supporting Information S1: Figure 11A), as confirmed by two-way ANOVA (Supporting Information S1: Table 25). In K562 we observed no sensitization to NHEJ inhibitors in sgPRDX1 cells. Moreover, both control and sgPRDX1 K562 cells were resistant to OLAP (Supporting Information S1: Figure 11B and Table 26).

In the next step, we assessed the effects of NHEJ inhibitors on the efficacy of IMAT in PRDX1-knockout cells. For both NHEJ inhibitors, the combinations with IMAT were more effective in BV173 sgPRDX1 cells than in sgNTC cells (Figure 6A and Supporting Information S1: Figure 12 and Tables 27 and 28). No such effects were observed in K562 cells (Supporting Information S1: Figure 13 and Tables 29 and 30). To further explore the lymphoid lineage specificity of these effects, we generated PRDX1 knockout in another Ph<sup>+</sup> BCP-ALL cell line, SUP-B15 (Supporting Information S1: Figure 14A). SUP-B15 sgPRDX1 cells

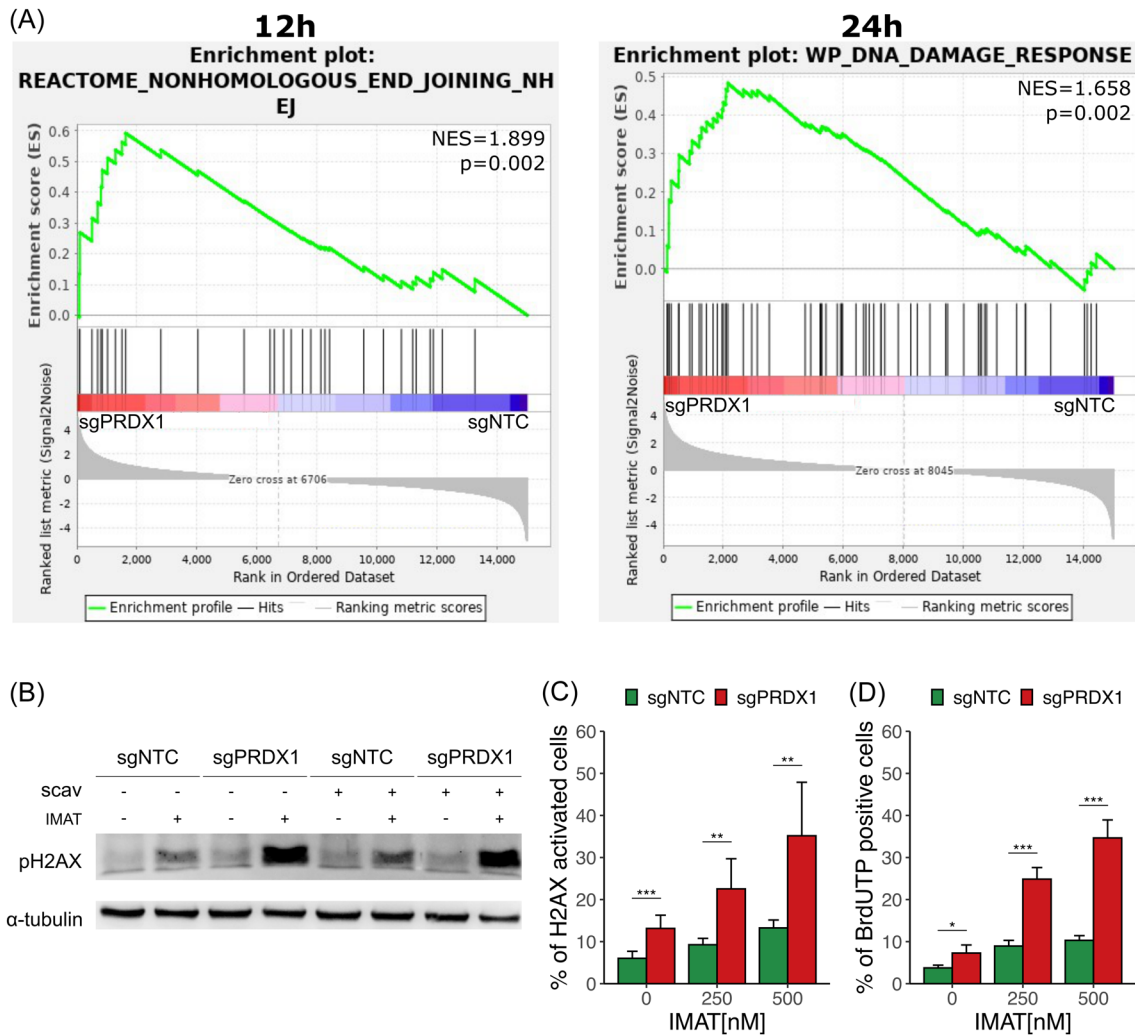


**FIGURE 5** Peroxiredoxin-1 (PRDX1) knockout triggers the upregulation of DNA damage response (DDR)-related gene sets and the accumulation of DNA lesions in lymphoid Philadelphia-positive (Ph<sup>+</sup>) cells treated with imatinib (IMAT). (A) Enrichment plots of RNA-sequencing (RNAseq) gene set enrichment analysis showing upregulation of nonhomologous end-joining (NHEJ) and DDR-related pathways in sgPRDX1 BV173 cells treated with 250 nM IMAT for 12 and 24 h, as compared to the corresponding IMAT-treated, sgNTC cells. (B) Activation of H2AX in BV173 sgPRDX1 and sgNTC cells upon treatment with 250 nM IMAT for 24 h were measured by immunoblot, using antibodies recognizing phosphorylated H2AX. (C) Activation of H2AX in BV173 sgPRDX1 cells upon treatment with the indicated concentration of IMAT for 24 h was measured by intracellular staining of pH2AX and assessment using Muse<sup>®</sup> H2AX Activation Dual Detection Kit. Means  $\pm$  SD are presented ( $n = 7$ ). Statistical significance was estimated by a two-way analysis of variance (ANOVA) with a post hoc pairwise  $t$ -test for each IMAT concentration separately. \*\* $p < 0.01$ ; \*\*\* $p < 0.001$ . (D) Measurement of double-stranded breaks in BV173 sgPRDX1 cells induced by 24 h IMAT treatment was assessed by terminal deoxynucleotidyl transferase dUTP nick-end labeling assay with flow cytometry. Means  $\pm$  SD are presented ( $n = 4$ ). Statistical significance was estimated by a two-way ANOVA with a post hoc pairwise  $t$ -test for each IMAT concentration separately. \* $p < 0.05$ ; \*\*\* $p < 0.001$ .

exhibited increased sensitivity to NEDI, IMAT, and their combinations compared to sgNTC cells (Figure 6B and Supporting Information S1: Table 31). Moreover, PRDX1 knockout significantly reduced the number of viable SUP-B15 cells (Supporting Information S1: Figure 14B and Table 32), affirming the observed effects in another Ph<sup>+</sup> lymphoid cell line.

Next, we investigated the effect of triple combinations involving the TXN system inhibitor AUR, IMAT, and one of two NHEJ inhibitors, NEDI or OLAP, in three Ph<sup>+</sup> lymphoid cell lines, BV173, SUP-B15 and TOM-1. In all the tested cell lines, the combinations of NHEJ inhibitors and IMAT showed high effectiveness, which was further improved by the addition of AUR (Figure 6C-E and Supporting Information S1: Figures 15-17 and Tables 33-36). Notably, the interactions among these two or three drugs were mostly synergistic, as indicated by a synergy score above 10 (see Figure 6C-E).

To investigate whether the observed cytotoxic effect of NEDI, AUR, and TKIs combinations is caused by the accumulation of DNA damage, we assessed the levels of DNA lesions. Rapid phosphorylation of H2AX was observed in cells treated with all three drugs for 6 h, and it was significantly higher than in any group treated with single drugs only (Figure 6F and Supporting Information S1: Table 37). Pronounced induction of DNA DSBs we also observed in cells treated with triple combination for 24 h using TUNEL assay (Figure 6G and Supporting Information S1: Table 38). However, it is important to note that in this case, the observed difference may be overestimated due to the concurrent detection of DNA fragmentation resulting from apoptosis.

Encouraged by these promising effects in cell lines, we tested the ex vivo efficacy of the triple combinations in six Ph<sup>+</sup> PDX (B-ALL and lyBP CML). As presented in Figure 7A, NEDI exerted cytotoxic effects



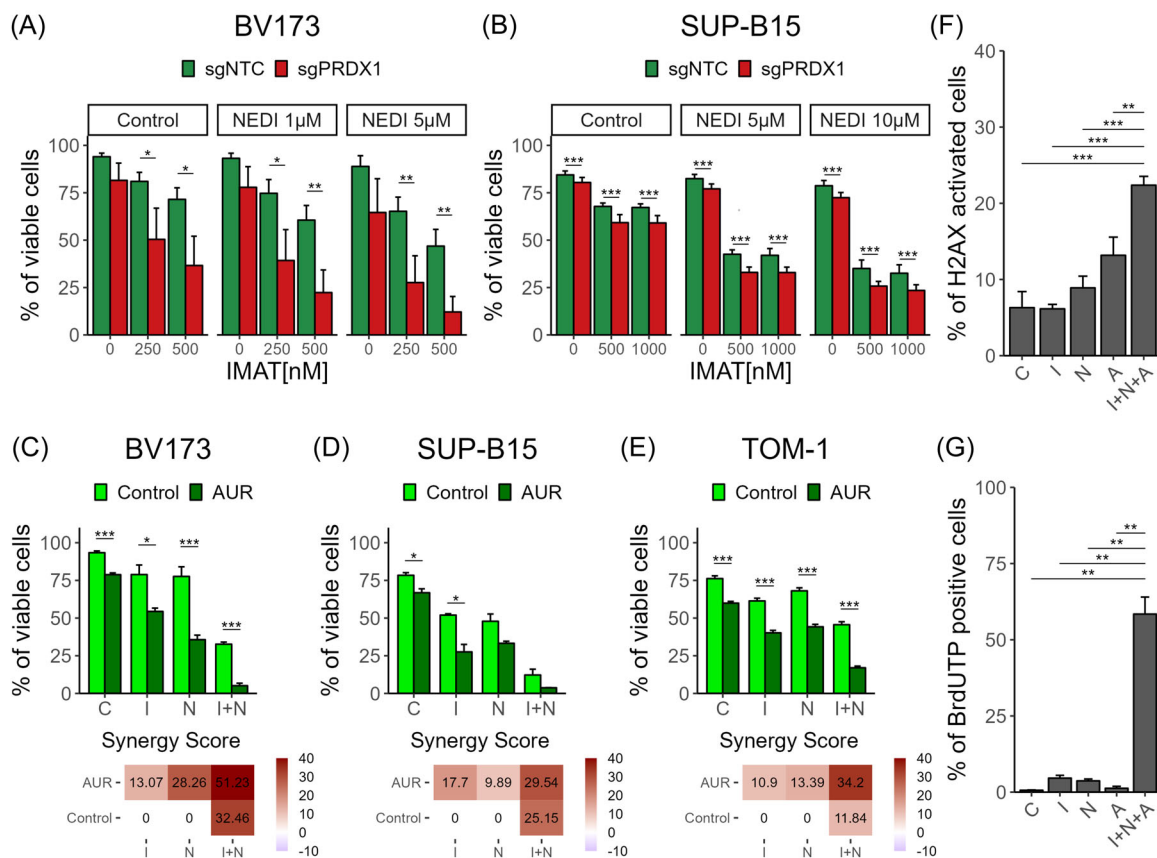


**FIGURE 6** Triple combination involving tyrosine kinase inhibitors (TKIs), inhibition of the thioredoxin (TXN) system, and nonhomologous end-joining (NHEJ) effectively kills Philadelphia-positive (Ph<sup>+</sup>) lymphoid cell lines. (A, B) Cytotoxic effects of 48 h imatinib (IMAT) and nedisertib (NEDI) combinations were measured in sgNTC and sgPRDX1 BV173 (A) and SUP-B15 (B) cells by propidium iodide (PI) staining and flow cytometry. Means  $\pm$  SD are presented (BV173  $n = 4$ ; SUP-B15 sgNTC  $n = 8$ ; sgPRDX1  $n = 12$ ). Statistical significance was calculated by a three-way analysis of variance (ANOVA) with a post hoc pairwise *t*-test. \* $p < 0.05$ ; \*\* $p < 0.01$ ; \*\*\* $p < 0.001$ . (C–E) Cytotoxic effects of triple combination including 10  $\mu$ M NEDI (N), 0.125  $\mu$ M (BV173 and SUP-B15) or 4  $\mu$ M (TOM-1) IMAT (I), and 0.125  $\mu$ M (BV173), 0.25  $\mu$ M (SUP-B15), or 1  $\mu$ M (TOM-1) auranofin (AUR) were assessed by PI staining and flow cytometry after 48 h of treatment in BV173 (C), SUP-B15 (D), and TOM-1 (E) cells. Means  $\pm$  SD are presented ( $n = 4$ ). Bliss synergy scores are presented below the corresponding plots. Statistical significance was calculated by a three-way ANOVA with a post hoc pairwise *t*-test. \* $p < 0.05$ ; \*\*\* $p < 0.001$ . (F) Activation of H2AX in BV173 cells upon 6 h treatment with 500 nM IMAT, 10  $\mu$ M NEDI, and 0.25  $\mu$ M AUR was measured by intracellular staining of pH2AX and assessment in flow cytometry using Muse<sup>®</sup> H2AX Activation Dual Detection Kit. Means  $\pm$  SD are presented ( $n = 4$ ). Statistical significance was estimated by a one-way ANOVA with a post hoc pairwise *t*-test with Bonferroni correction. \*\* $p < 0.01$ ; \*\*\* $p < 0.001$ . (G) Measurement of DNA double-stranded breaks in BV173 cells induced by 500 nM IMAT, 10  $\mu$ M NEDI, and 0.25  $\mu$ M AUR treatment was assessed by TUNEL assay with flow cytometry. Means  $\pm$  SD are presented ( $n = 4$ ). Statistical significance was estimated by a one-way ANOVA with a post hoc pairwise *t*-test with Bonferroni correction. \*\* $p < 0.01$ .

when used as a single drug or in combination with IMAT and DASA. Moreover, the addition of AUR significantly enhanced the efficacy of both TKIs, NEDI, and their combinations (Supporting Information S1: Table 39), in concentrations lower than reported human serum  $C_{max}$  values.<sup>46–49</sup> Synergistic effects of triple combinations were observed in PDX#1, PDX#2, and PDX#3, while additive effects were seen in PDX#4, and PDX#5 (Figure 7A). PDX#6 was particularly sensitive to AUR, which could explain the lack of additional enhancement of cytotoxicity due to the addition of TKIs or NEDI (Figure 7A). Similar results were also obtained using primary lymphoblasts isolated from a Ph<sup>+</sup> B-ALL patient (Supporting Information S1: Figure 18 and Table 40). In contrast, OLAP was ineffective in all tested combinations (Supporting Information S1: Figure 19 and Table 41). Next, we assessed the cytotoxicity of TKIs, NEDI, and AUR combinations against normal CD19<sup>+</sup> cells isolated from healthy donors' peripheral blood (Figure 7B and Supporting Information S1: Table 42). Albeit mild cytotoxicity of combinations involving DASA was observed, AUR

addition did not significantly enhance these cytotoxic effects (Supporting Information S1: Table 42). The comparative analysis of the cytotoxic effects of the combinations against leukemic and normal CD19<sup>+</sup> cells revealed that NEDI and its combinations with TKIs and AUR were more cytotoxic toward leukemic than normal CD19<sup>+</sup> cells (Figure 7C and Supporting Information S1: Table 43), indicating tumor cell selectivity.

These results reveal a potent cytotoxic effect of drug combinations composed of TKIs, NHEJ inhibitors, and AUR against Ph<sup>+</sup> B-ALL, particularly those containing cNHEJ inhibitor—NEDI.

## DISCUSSION

Although the introduction of TKIs for the treatment of Ph<sup>+</sup> B-ALL has improved the prognosis of patients, the significant fraction of relapses warrants further search for new therapeutic targets. As in Ph<sup>+</sup> B-ALL

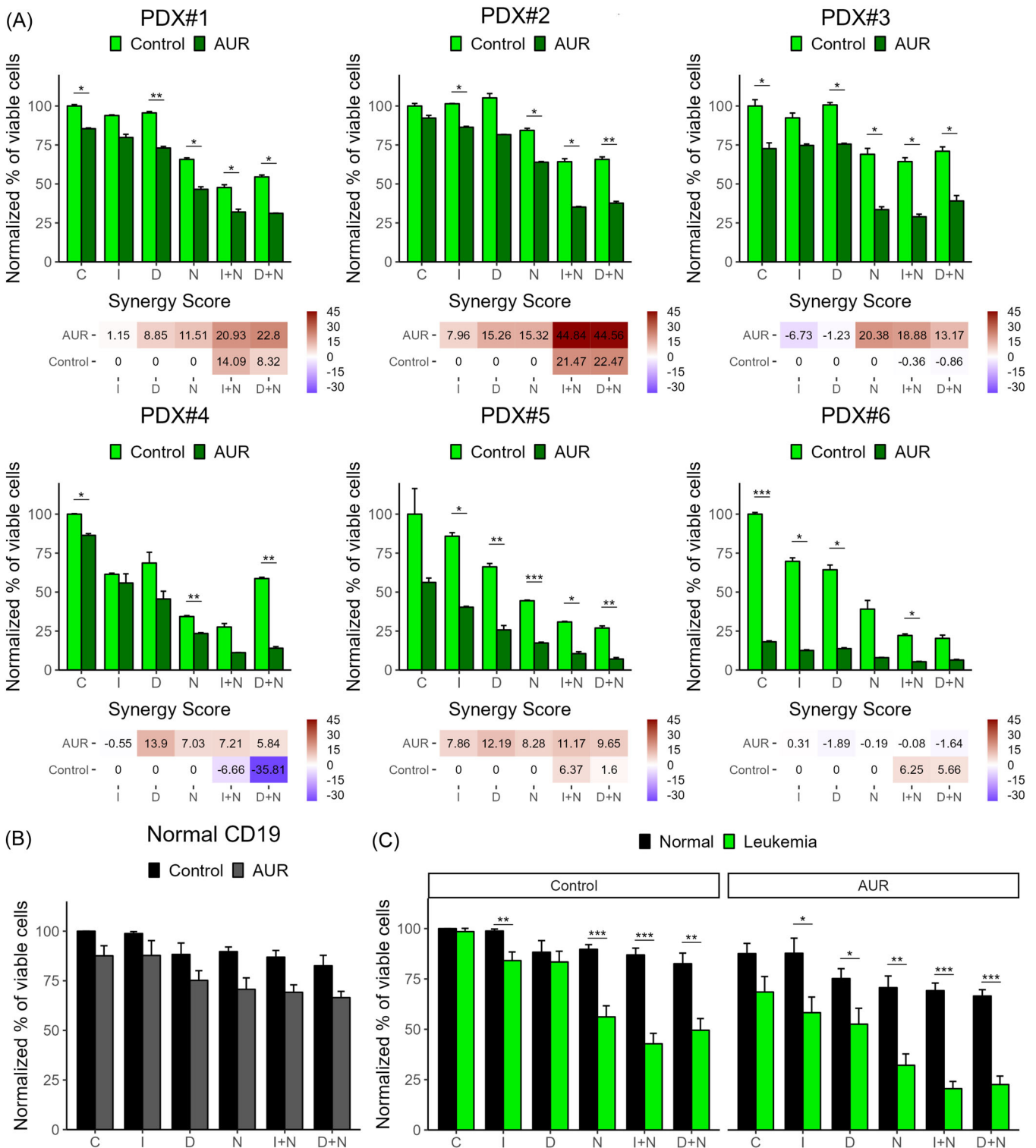


**FIGURE 7** Triple combination of tyrosine kinase inhibitors (TKIs), auranofin (AUR), and nedisertib (NEDI) has a robust and selective effect on Philadelphia-positive (Ph<sup>+</sup>) BCP-ALL patient-derived xenograft (PDX) cells. (A) Cytotoxic effects of triple combination including 10  $\mu$ M NEDI (N), 8  $\mu$ M imatinib (IMAT) (I) or 160 nM dasatinib (DASA) (D), and 0.25  $\mu$ M AUR were assessed by propidium iodide (PI) staining and flow cytometry after 72 h of treatment of six Ph<sup>+</sup> PDXs ( $n = 2$ ). For each PDX, the mean viability from two biological repeats was normalized to the mean viability of untreated cells. Means  $\pm$  SD are presented. Bliss synergy scores are presented below the corresponding plots. Statistical significance was calculated by a paired three-way ANOVA with a post hoc pairwise paired  $t$ -test. \* $p < 0.05$ ; \*\* $p < 0.01$ ; \*\*\* $p < 0.001$ . (B) Cytotoxic effects of triple combination including 10  $\mu$ M NEDI (N), 8  $\mu$ M IMAT (I) or 160 nM DASA (D), and 0.25  $\mu$ M AUR were assessed by PI staining and flow cytometry after 48 h of treatment of CD19<sup>+</sup> cells isolated from three healthy donors' PBMC. For each donor, the mean viability from two or three biological repeats was normalized to the mean viability of untreated cells and then aggregated. Means  $\pm$  SD are presented ( $n = 3$ ). Statistical significance was calculated by a three-way ANOVA with a post hoc pairwise paired  $t$ -test. No significant differences were found. (C) Comparison of 0.25  $\mu$ M AUR, 10  $\mu$ M NEDI (N), and either 8  $\mu$ M IMAT (I) or 160 nM DASA (D) combination effect on normal CD19<sup>+</sup> and leukemic cells. Data presented on the graph are extracted from panels A and B. The viability of leukemic samples is pooled from all six tested PDXs for comparison. Statistical significance was calculated by a one-way ANOVA with a post hoc pairwise  $t$ -test. \* $p < 0.05$ ; \*\* $p < 0.01$ ; \*\*\* $p < 0.001$ .

patients, TKIs are only effective when combined with multiagent chemotherapy, more selective drugs that could potentiate TKIs are particularly needed. In this work, we present the lymphoid-specific role of PRDX1, one of the elements of the TXN system, in viability and sensitivity to TKIs of Ph<sup>+</sup> leukemias. We show that inhibition of the TXN system as well as the knockout of PRDX1 diminish the viability of Ph<sup>+</sup> B-ALL cells and sensitize them to TKIs. In addition, we observe the cytotoxicity of NHEJ inhibitors against Ph<sup>+</sup> B-ALL cells and that this cytotoxicity could be further enhanced by the inhibition of the TXN system. Finally, we show the high in vitro efficacy of the triple combinations comprising inhibitors of the TXN system, NHEJ DNA repair pathways, and TKIs against Ph<sup>+</sup> B-ALL. Importantly, these combinations have exhibited high effectiveness at clinically relevant concentrations achievable in plasma.

The TXN system was shown to support therapy resistance and survival of B-cell malignancies before<sup>10,50</sup>; hence, it was chosen as a potential target in Ph<sup>+</sup> B-ALL in our study. The overexpression of selected elements of the TXN system was previously seen in various cancer types.<sup>44,51</sup> Herein, we found the upregulation of only PRDX1 in Ph<sup>+</sup> lymphoid cells, compared to their Ph<sup>+</sup> myeloid counterparts, while the other elements of the TXN system were downregulated. As PRDX1 needs TXN1 for its catalytic function,<sup>52</sup> lower TXN1 expression might limit the antioxidant activity of PRDX1. Together with our observation that sensitization of PRDX1-knockout cells to TKIs is not strictly ROS-dependent, this suggests a more complex role of PRDX1 in lymphoid cells, beyond ROS-scavenging, as was seen before in solid tumors.<sup>53</sup> In this study, we show for the first time that the lack of PRDX1 increases the sensitivity of Ph<sup>+</sup> B-ALL to TKIs and we demonstrate the synergistic effects of TXN system inhibitors with TKIs. Furthermore, based on the RNAseq analysis of PRDX1-deficient cells treated with IMAT, we identify DDR pathways as a novel vulnerability of Ph<sup>+</sup> B-ALL cells. We demonstrate that PRDX1-deficient B-ALL cells treated with IMAT accumulate greater amounts of DNA lesions and are more susceptible to inhibitors of NHEJ. Based on these studies, we propose novel triple combinations consisting of the TXN inhibitors, TKIs, and NHEJ inhibitors, and show their efficacy in preclinical models of Ph<sup>+</sup> B-ALL. The triple combinations cause rapid accumulation of DNA damage and induce death of Ph<sup>+</sup> B-ALL cells. Even though those combinations exerted mild cytotoxic effects on the normal CD19<sup>+</sup> cells, a combination of NEDI, IMAT, and AUR killed leukemic cells more effectively. These promising in vitro results warrant further in vivo evaluation.

Another important finding presented in this work is the sensitivity of Ph<sup>+</sup> lymphoid cells to altNHEJ and cNHEJ inhibitors, OLAP and NEDI, which are promising and relatively selective anticancer drugs. Among altNHEJ inhibitors, PARP1 inhibitors are clinically approved for the treatment of ovarian, breast, and recently also pancreatic and prostate cancers with deficiencies in DDR pathways.<sup>54-57</sup> Inhibitors of cNHEJ, molecularly targeting mainly DNA-PK, are now tested in clinical trials as possible anticancer agents (NCT03983824, NCT03983824, and NCT02977780). The cytotoxic effects of OLAP and other PARP1 inhibitors against primary CML cells have been presented before and were attributed to BCR::ABL1-mediated downregulation of BRCA1, DNA-PK, and other enzymes involved in DNA repair. Moreover, OLAP potentiated the effects of IMAT and ponatinib in CML and Ph<sup>+</sup> B-ALL primary cells.<sup>26</sup> On the other hand, very few studies showed the antileukemic activity of cNHEJ inhibitors.<sup>58,59</sup> Herein, we show that NEDI, but not OLAP, exerts cytotoxic effects against Ph<sup>+</sup> B-ALL PDX cells and enhances the activity of TKIs, while both NEDI and OLAP are similarly potent in Ph<sup>+</sup> B-ALL cell lines. Even though this indicates the more prominent role of cNHEJ for the viability of primary Ph<sup>+</sup> lymphoid cells, it is important to mention that these cells do not proliferate in vitro. Although it was demonstrated that OLAP can be active against quiescent,

nonproliferating cells,<sup>26</sup> altNHEJ is preferentially active in dividing cells,<sup>60,61</sup> which may explain the lack of OLAP activity in ex vivo assays. As B-ALL PDX cells proliferate in vivo, further studies in animal models are needed to properly evaluate OLAP efficacy toward Ph<sup>+</sup> B-ALL PDX.

Notably, we observed that the leukemia-promoting role of PRDX1 is lineage-specific. We showed that Ph<sup>+</sup> lymphoid cells are sensitive to the TXN system inhibitors and that PRDX1 knockout diminished their viability and sensitized Ph<sup>+</sup> lymphoid cells to TKIs and NHEJ inhibitors, while no such effects were observed in Ph<sup>+</sup> myeloid cells. Specific vulnerabilities of Ph<sup>+</sup> leukemias associated with lymphoid lineage have been presented before.<sup>62-64</sup> Notably, in contrast to CML, Ph<sup>+</sup> B-ALL cells were shown to be dependent on the generation of NADPH and the expression of antioxidant enzymes.<sup>65</sup> Furthermore, lymphoid cells express recombinase-activating genes that are involved in the generation of DSBs during immunoglobulin gene rearrangements.<sup>66</sup> Hence, Ph<sup>+</sup> lymphoid cells could be more sensitive to redox imbalance and dependent on constant activation of DDR pathways. Further studies are needed to elucidate the mechanisms behind the lymphoid-specific effects of the TXN system.

In conclusion, this study revealed that the TXN system and PRDX1 play a specific role in Ph<sup>+</sup> lymphoid leukemias, having a significant impact on the efficiency of DNA repair in these cells, especially after treatment with TKIs. This allowed for the discovery of a novel combination of AUR and NHEJ inhibitors, which might be a promising therapeutic strategy in Ph<sup>+</sup> B-ALL for further preclinical and clinical studies.

## ACKNOWLEDGMENTS

We gratefully acknowledge all patients, their parents, and staff from the Central Clinical Hospital of the Medical University of Lodz, and from the Institute of Hematology and Transfusion Medicine in Warsaw. We also thank Monika Pepek, Elzbieta Gutowska, and Karolina Siudakowska from the Department of Immunology at the Medical University of Warsaw for their help and support throughout the project.

## AUTHOR CONTRIBUTIONS

Lukasz Komorowski, Agata Pastorczak, and Malgorzata Firczuk conceived the experimental design. Lukasz Komorowski, Agnieszka Dabkowska, Joanna Madzio, Agata Pastorczak, Kacper Szczygiel, Martyna Janowska, Klaudyna Fidy, Jaromir Hunia, Malgorzata Bajor, and Malgorzata Firczuk performed and analyzed experiments. Lukasz Komorowski, Joanna Madzio, Agata Pastorczak, Magdalena Winiarska, Malgorzata Bajor, and Malgorzata Firczuk curated the data. Lukasz Komorowski, Joanna Madzio, Agata Pastorczak, Martyna Janowska, Klaudyna Fidy, Maksymilian Bielecki, Jaromir Hunia, Malgorzata Bajor, Agnieszka Dabkowska, Tomasz Stoklosa, Magdalena Winiarska, and Malgorzata Firczuk analyzed and interpreted the data. Maksymilian Bielecki consulted and reviewed all of the statistical analyses and was involved in the preparation of the manuscript. Agata Pastorczak, Joanna Madzio, Tomasz Stoklosa, and Elzbieta Patkowska recruited patients, collected patients' material, and provided clinical data. Malgorzata Firczuk and Lukasz Komorowski wrote the original manuscript. All authors critically reviewed and edited the manuscript. Malgorzata Firczuk coordinated the whole project, supervised the experimental design, consulted the obtained results, and provided funding.

## CONFLICT OF INTEREST STATEMENT

The authors declare no conflict of interest.

## DATA AVAILABILITY STATEMENT

The data that support the findings of this study are available from the corresponding author upon reasonable request.

## FUNDING

This work was supported by the National Science Centre (Poland) grants: 2015/18/E/NZ5/00723 (M. F.) and 2019/35/B/NZ5/01428 (M. F.). K. F. was supported by the Foundation for Polish Science (FNP).

## ORCID

Lukasz Komorowski  <https://orcid.org/0000-0002-7646-1968>

## SUPPORTING INFORMATION

Additional supporting information can be found in the online version of this article.

## REFERENCES

- Perrotti D, Jamieson C, Goldman J, Skorski T. Chronic myeloid leukemia: mechanisms of blastic transformation. *J Clin Invest*. 2010;120(7):2254-2264. doi:10.1172/JCI41246
- Hunger SP, Mullighan CG. Redefining ALL classification: toward detecting high-risk ALL and implementing precision medicine. *Blood*. 2015;125(26):3977-3987. doi:10.1182/blood-2015-02-580043
- Yeung DTO, Osborn MP, White DL. B-cell acute lymphoblastic leukaemia: recent discoveries in molecular pathology, their prognostic significance, and a review of the current classification. *Br J Haematol*. 2022;197(1):13-27. doi:10.1111/bjh.17879
- Reid AG, De Melo VA, Elderfield K, et al. Phenotype of blasts in chronic myeloid leukemia in blastic phase—analysis of bone marrow trephine biopsies and correlation with cytogenetics. *Leuk Res*. 2009;33(3):418-425. doi:10.1016/j.leukres.2008.07.019
- Branford S, Wang P, Yeung DT, et al. Integrative genomic analysis reveals cancer-associated mutations at diagnosis of CML in patients with high-risk disease. *Blood*. 2018;132(9):948-961. doi:10.1182/blood-2018-02-832253
- Adnan Awad S, Kankainen M, Ojala T, et al. Mutation accumulation in cancer genes relates to nonoptimal outcome in chronic myeloid leukemia. *Blood Adv*. 2020;4(3):546-559. doi:10.1182/bloodadvances.2019000943
- Fielding AK. Curing Ph<sup>+</sup> ALL: assessing the relative contributions of chemotherapy, TKIs, and allogeneic stem cell transplant. *Hematology*. 2019;2019(1):24-29. doi:10.1182/hematology.2019000010
- Sattler M, Verma S, Shrikhande G, et al. The BCR/ABL tyrosine kinase induces production of reactive oxygen species in hematopoietic cells. *J Biol Chem*. 2000;275(32):24273-24278. doi:10.1074/jbc.M002094200
- Naughton R, Quiney C, Turner SD, Cotter TG. Bcr-Abl-mediated redox regulation of the PI3K/AKT pathway. *Leukemia*. 2009;23(8):1432-1440. doi:10.1038/leu.2009.49
- Fidyk K, Pastorczak A, Goral A, et al. Targeting the thioredoxin system as a novel strategy against B-cell acute lymphoblastic leukemia. *Mol Oncol*. 2019;13(5):1180-1195. doi:10.1002/1878-0261.12476
- Graczyk-Jarzynka A, Goral A, Muchowicz A, et al. Inhibition of thioredoxin-dependent H<sub>2</sub>O<sub>2</sub> removal sensitizes malignant B-cells to pharmacological ascorbate. *Redox Biol*. 2019;21:101062. doi:10.1016/j.redox.2018.11.020
- Wang J, Wang J, Lopez E, et al. Repurposing auranofin to treat TP53-mutated or PTEN-deleted refractory B-cell lymphoma. *Blood Cancer J*. 2019;9(12):95. doi:10.1038/s41408-019-0259-8
- Hou GX, Liu PP, Zhang S, et al. Elimination of stem-like cancer cell side-population by auranofin through modulation of ROS and glycolysis. *Cell Death Dis*. 2018;9(2):89. doi:10.1038/s41419-017-0159-4
- Abdalbari FH, Goyeneche AA, Martinez-Jaramillo E, Sabri S, Telleria CM. Abstract 1014: repurposing the anti-rheumatic gold compound auranofin for high-grade serous ovarian cancer therapy. *Cancer Res*. 2021;81(13\_suppl):1014. doi:10.1158/1538-7445.AM2021-1014
- Krishnamurthy D, Karver MR, Fiorillo E, et al. Gold(I)-mediated inhibition of protein tyrosine phosphatases: a detailed in vitro and cellular study. *J Med Chem*. 2008;51(15):4790-4795. doi:10.1021/jm800101w
- Liu N, Li X, Huang H, et al. Clinically used antirheumatic agent auranofin is a proteasomal deubiquitinase inhibitor and inhibits tumor growth. *Oncotarget*. 2014;5(14):5453-5471. doi:10.18632/oncotarget.2113
- Fiskus W, Saba N, Shen M, et al. Auranofin induces lethal oxidative and endoplasmic reticulum stress and exerts potent preclinical activity against chronic lymphocytic leukemia. *Cancer Res*. 2014;74(9):2520-2532. doi:10.1158/0008-5472.CAN-13-2033
- Zhang X, Selvaraju K, Saei AA, et al. Repurposing of auranofin: thioredoxin reductase remains a primary target of the drug. *Biochimie*. 2019;162:46-54. doi:10.1016/j.biochi.2019.03.015
- Gromer S, Arscott LD, Williams CH, Schirmer RH, Becker K. Human placenta thioredoxin reductase: isolation of the selenoenzyme, steady state kinetics, and inhibition by therapeutic gold compounds. *J Biol Chem*. 1998;273(32):20096-20101. doi:10.1074/jbc.273.32.20096
- O'Connor MJ. Targeting the DNA damage response in cancer. *Mol Cell*. 2015;60(4):547-560. doi:10.1016/j.molcel.2015.10.040
- Huang R, Zhou PK. DNA damage repair: historical perspectives, mechanistic pathways and clinical translation for targeted cancer therapy. *Signal Transduct Target Ther*. 2021;6(1):254. doi:10.1038/s41392-021-00648-7
- Podszycalow-Bartnicka P, Wolczyk M, Kusio-Kobialka M, et al. Downregulation of BRCA1 protein in BCR-ABL1 leukemia cells depends on stress-triggered TIAR-mediated suppression of translation. *Cell Cycle*. 2014;13(23):3727-3741. doi:10.4161/15384101.2014.965013
- Deutsch E, Dugray A, AbdulKarim B, et al. BCR-ABL down-regulates the DNA repair protein DNA-PKcs. *Blood*. 2001;97(7):2084-2090. doi:10.1182/blood.V97.7.2084
- Choudhury A, Zhao H, Jalali F, et al. Targeting homologous recombination using imatinib results in enhanced tumor cell chemosensitivity and radiosensitivity. *Mol Cancer Ther*. 2009;8(1):203-213. doi:10.1158/1535-7163.MCT-08-0959
- Slupianek A, Poplawski T, Jozwiakowski SK, et al. BCR/ABL stimulates WRN to promote survival and genomic instability. *Cancer Res*. 2011;71(3):842-851. doi:10.1158/0008-5472.CAN-10-1066
- Nieborowska-Skorska M, Sullivan K, Dasgupta Y, et al. Gene expression and mutation-guided synthetic lethality eradicates proliferating and quiescent leukemia cells. *J Clin Invest*. 2017;127(6):2392-2406. doi:10.1172/JCI90825
- Al-Aamri HM, Irving HR, Meehan-Andrews T, Bradley C. Determination of the DNA repair pathways utilised by acute lymphoblastic leukaemia cells following daunorubicin treatment. *BMC Res Notes*. 2019;12(1):625. doi:10.1186/s13104-019-4663-8
- R Core Team. *R: A Language and Environment for Statistical Computing*. R Foundation for Statistical Computing; 2022. <https://www.R-project.org/>
- Muchowicz A, Firczuk M, Chlebowska J, et al. Adenanthin targets proteins involved in the regulation of disulphide bonds. *Biochem Pharmacol*. 2014;89(2):210-216. doi:10.1016/j.bcp.2014.02.022
- Zheng S, Wang W, Aldahdooh J, et al. SynergyFinder Plus: toward better interpretation and annotation of drug combination screening datasets. *Genomics Insights*. 2022;20:587-596. doi:10.1016/j.gpb.2022.01.004
- Cao Z, Budinich KA, Huang H, et al. ZMYND8-regulated IRF8 transcription axis is an acute myeloid leukemia dependency. *Mol Cell*. 2021;81(17):3604-3622.e10. doi:10.1016/j.molcel.2021.07.018
- Tanaka N, Wang YH, Shiseki M, Takanashi M, Motoji T. Inhibition of PRAME expression causes cell cycle arrest and apoptosis in leukemic cells. *Leuk Res*. 2011;35(9):1219-1225. doi:10.1016/j.leukres.2011.04.005



33. Zhang T, Yang J, Vaikari VP, et al. Apolipoprotein C2–CD36 promotes leukemia growth and presents a targetable axis in acute myeloid leukemia. *Blood Cancer Discov.* 2020;1(2):198-213. doi:10.1158/2643-3230.BCD-19-0077
34. Adane B, Ye H, Khan N, et al. The hematopoietic oxidase NOX2 regulates self-renewal of leukemic stem cells. *Cell Rep.* 2019;27(1):238-254.e6. doi:10.1016/j.celrep.2019.03.009
35. Voeltzel T, Flores-Violante M, Zylbersztejn F, et al. A new signaling cascade linking BMP4, BMPR1A, ΔNp73 and NANOG impacts on stem-like human cell properties and patient outcome. *Cell Death Dis.* 2018;9(10):1011. doi:10.1038/s41419-018-1042-7
36. Nayak RC, Hegde S, Althoff MJ, et al. The signaling axis atypical protein kinase C $\lambda$ /t-Satb2 mediates leukemic transformation of B-cell progenitors. *Nat Commun.* 2019;10(1):46. doi:10.1038/s41467-018-07846-y
37. Zhang T, Zhou J, Zhang W, et al. H19 overexpression promotes leukemogenesis and predicts unfavorable prognosis in acute myeloid leukemia. *Clin Epigenet.* 2018;10(1):47. doi:10.1186/s13148-018-0486-z
38. Bras S, Martin-Lannerée S, Gobert V, et al. Myeloid leukemia factor is a conserved regulator of RUNX transcription factor activity involved in hematopoiesis. *Proc Natl Acad Sci USA.* 2012;109(13):4986-4991. doi:10.1073/pnas.1117317109
39. Baumann AMT, Bakkers MJG, Buettner FFR, et al. 9-O-Acetylation of sialic acids is catalysed by CASD1 via a covalent acetyl-enzyme intermediate. *Nat Commun.* 2015;6(1):7673. doi:10.1038/ncomms8673
40. Fenouille N, Puissant A, Dufies M, et al. Persistent activation of the Fyn/ERK kinase signaling axis mediates imatinib resistance in chronic myelogenous leukemia cells through upregulation of intracellular SPARC. *Cancer Res.* 2010;70(23):9659-9670. doi:10.1158/0008-5472.CAN-10-2034
41. Miyagawa Y, Matsushita Y, Suzuki H, et al. Frequent downregulation of LRRC26 by epigenetic alterations is involved in the malignant progression of triple-negative breast cancer. *Int J Oncol.* 2018;52:1539-1558. doi:10.3892/ijo.2018.4301
42. Grasso S, Cangelosi D, Chapelle J, et al. The SRCIN1/p140Cap adaptor protein negatively regulates the aggressiveness of neuroblastoma. *Cell Death Differ.* 2020;27(2):790-807. doi:10.1038/s41418-019-0386-6
43. Poet GJ, Oka OB, van Lith M, et al. Cytosolic thioredoxin reductase 1 is required for correct disulfide formation in the ER. *EMBO J.* 2017;36(5):693-702. doi:10.15252/embj.201695336
44. Trzeciecka A, Klossowski S, Bajor M, et al. Dimeric peroxiredoxins are druggable targets in human Burkitt lymphoma. *Oncotarget.* 2016;7(2):1717-1731. doi:10.18632/oncotarget.6435
45. Mohammad A, Saini RV, Kumar R, et al. A curious case of cysteines in human peroxiredoxin I. *Redox Biol.* 2020;37:101738. doi:10.1016/j.redox.2020.101738
46. von Mehren M, Widmer N. Correlations between imatinib pharmacokinetics, pharmacodynamics, adherence, and clinical response in advanced metastatic gastrointestinal stromal tumor (GIST): an emerging role for drug blood level testing? *Cancer Treat Rev.* 2011;37(4):291-299. doi:10.1016/j.ctrv.2010.10.001
47. Lilly MB, Ottmann OG, Shah NP, et al. Dasatinib 140 mg once daily versus 70 mg twice daily in patients with Ph-positive acute lymphoblastic leukemia who failed imatinib: results from a phase 3 study. *Am J Hematol.* 2010;85(3):164-170. doi:10.1002/ajh.21615
48. Van Bussel MTJ, Awada A, De Jonge MJA, et al. A first-in-man phase 1 study of the DNA-dependent protein kinase inhibitor peposertib (formerly M3814) in patients with advanced solid tumours. *Br J Cancer.* 2021;124(4):728-735. doi:10.1038/s41416-020-01151-6
49. Bundred N, Gardovskis J, Jaskiewicz J, et al. Evaluation of the pharmacodynamics and pharmacokinetics of the PARP inhibitor olaparib: a phase I multicentre trial in patients scheduled for elective breast cancer surgery. *Invest New Drugs.* 2013;31(4):949-958. doi:10.1007/s10637-012-9922-7
50. Fidyk K, Pastorczak A, Cyran J, et al. Potent, p53-independent induction of NOXA sensitizes MLL-rearranged B-cell acute lymphoblastic leukemia cells to venetoclax. *Oncogene.* 2022;41(11):1600-1609. doi:10.1038/s41388-022-02196-y
51. Lincoln DT, Ali Emadi EM, Tonissen KF, Clarke FM. The thioredoxin–thioredoxin reductase system: over-expression in human cancer. *Anticancer Res.* 2003;23(3B):2425-2433.
52. Xie W, Ma W, Liu P, Zhou F. Overview of thioredoxin system and targeted therapies for acute leukemia. *Mitochondrion.* 2019;47:38-46. doi:10.1016/j.mito.2019.04.010
53. Kim YJ, Lee WS, Ip C, Chae HZ, Park EM, Park YM. Prx1 suppresses radiation-induced c-Jun NH2-terminal kinase signaling in lung cancer cells through interaction with the glutathione S-transferase Pi/c-Jun NH2-terminal kinase complex. *Cancer Res.* 2006;66(14):7136-7142. doi:10.1158/0008-5472.CAN-05-4446
54. European Medicines Agency. *Zejula*. EMA; 2018. <https://www.ema.europa.eu/en/medicines/human/EPAR/zejula>
55. European Medicines Agency. *Rubraca*. EMA; 2018. <https://www.ema.europa.eu/en/medicines/human/EPAR/rubraca>
56. European Medicines Agency. *Talzenna*. EMA; 2019. <https://www.ema.europa.eu/en/medicines/human/EPAR/talzenna>
57. European Medicines Agency. *Lynparza*. EMA; 2018. <https://www.ema.europa.eu/en/medicines/human/EPAR/lynparza>
58. Thijsen R, Ter Burg J, Garrick B, et al. Dual TORC/DNA-PK inhibition blocks critical signaling pathways in chronic lymphocytic leukemia. *Blood.* 2016;128(4):574-583. doi:10.1182/blood-2016-02-700328
59. Alikarami F, Safa M, Faranoush M, Hayat P, Kazemi A. Inhibition of DNA-PK enhances chemosensitivity of B-cell precursor acute lymphoblastic leukemia cells to doxorubicin. *Biomed Pharmacother.* 2017;94:1077-1093. doi:10.1016/j.biopha.2017.08.022
60. Yu W, Lescale C, Babin L, et al. Repair of G1 induced DNA double-strand breaks in S-G2/M by alternative NHEJ. *Nat Commun.* 2020;11(1):5239. doi:10.1038/s41467-020-19060-w
61. Hustedt N, Durocher D. The control of DNA repair by the cell cycle. *Nat Cell Biol.* 2017;19(1):1-9. doi:10.1038/ncb3452
62. Shojaee S, Chan LN, Buchner M, et al. PTEN opposes negative selection and enables oncogenic transformation of pre-B cells. *Nat Med.* 2016;22(4):379-387. doi:10.1038/nm.4062
63. Chen Z, Shojaee S, Buchner M, et al. Signalling thresholds and negative B-cell selection in acute lymphoblastic leukaemia. *Nature.* 2015;521(7552):357-361. doi:10.1038/nature14231
64. Komorowski L, Fidyk K, Patkowska E, Firczuk M. Philadelphia Chromosome-positive leukemia in the lymphoid lineage—similarities and differences with the myeloid lineage and specific vulnerabilities. *Int J Mol Sci.* 2020;21(16):5776. doi:10.3390/ijms21165776
65. Xiao G, Chan LN, Klemm L, et al. B-cell-specific diversion of glucose carbon utilization reveals a unique vulnerability in B cell malignancies. *Cell.* 2018;173(2):470-484.e18. doi:10.1016/j.cell.2018.02.048
66. Mullighan CG, Miller CB, Radtke I, et al. BCR–ABL1 lymphoblastic leukaemia is characterized by the deletion of Ikaros. *Nature.* 2008;453(7191):110-114. doi:10.1038/nature06866